



THE UNIVERSITY *of* EDINBURGH

Edinburgh Research Explorer

Fire Resistance Tests on Thin CFRP Prestressed Concrete Slabs

Citation for published version:

Maluk, C, Terrasi, GP, Bisby, L, Stutz, A & Hugi, E 2015, 'Fire Resistance Tests on Thin CFRP Prestressed Concrete Slabs', *Construction and Building Materials*, vol. 101, no. Part 1, pp. 558–571.
<https://doi.org/10.1016/j.conbuildmat.2015.10.031>

Digital Object Identifier (DOI):

[10.1016/j.conbuildmat.2015.10.031](https://doi.org/10.1016/j.conbuildmat.2015.10.031)

Link:

[Link to publication record in Edinburgh Research Explorer](#)

Document Version:

Peer reviewed version

Published In:

Construction and Building Materials

General rights

Copyright for the publications made accessible via the Edinburgh Research Explorer is retained by the author(s) and / or other copyright owners and it is a condition of accessing these publications that users recognise and abide by the legal requirements associated with these rights.

Take down policy

The University of Edinburgh has made every reasonable effort to ensure that Edinburgh Research Explorer content complies with UK legislation. If you believe that the public display of this file breaches copyright please contact openaccess@ed.ac.uk providing details, and we will remove access to the work immediately and investigate your claim.



1 **Fire Resistance Tests on Thin CFRP Prestressed Concrete Slabs**

2 Cristian Maluk^{1,*}, Giovanni Pietro Terrasi², Luke Bisby¹, Alex Stutz², Erich Hugi²

3 ¹ School of Engineering, The University of Edinburgh, UK

4 ² Empa, Swiss Federal Laboratories for Material Science and Technology, Switzerland

5 **Abstract**

6 Optimized, high-performance concrete elements, prestressed with carbon fibre reinforced
7 polymer (CFRP) tendons offer great potential within the sustainable modern built
8 environment. However, the performance of these elements in fire is not well known and must
9 be better understood for applications where fire resistance is required. Findings from large-
10 scale fire resistance tests on thin CFRP prestressed concrete slabs are presented and
11 discussed. Results show that explosive spalling in fire results in sudden collapse, and when
12 spalling is avoided failure occurs by loss of anchorage, which is in turn governed by the
13 temperature of the tendons.

14 **Keywords**

15 Carbon fibre reinforced polymer; precast concrete; prestressing; furnace testing; fire
16 resistance; heat-induced concrete spalling; loss of anchorage

17

* Corresponding Author

Currently at: School of Civil Engineering, The University of Queensland, Australia

Address: School of Civil Engineering, The University of Queensland, Brisbane QLD 4072, Australia

Email: c.maluk@uq.edu.au

Tel: +61 7 3365 3518

18 **1 INTRODUCTION & BACKGROUND**

19 Driven by the need for more durable and sustainable concrete structures; careful selection,
20 design, and optimization of concrete mixes and reinforcing materials used are now
21 commonplace in the precast concrete industry. Concrete elements incorporating high-
22 performance, self-consolidating concrete (HPSCC) and novel reinforcing and prestressing
23 materials, such as carbon fibre reinforced polymer (CFRP) tendons are one such example [1].
24 The application of thin-walled elements as façade beams and columns in building envelopes
25 (see Figure 1) shows the potential of these structural elements to be widely used in the
26 modern built environment.



27

28 **Figure 1 – Application of CFRP prestressed concrete L-shaped beams for structural façade elements in**
29 **Zurich, Switzerland [1].**

30

31 The combined use of CFRP and HPSCC enables the design of optimized, low-weight
32 prestressed elements with a reduced concrete cover and overall thickness [2, 3]; this gives
33 excellent serviceability (corrosion resistance, high stiffness and fatigue strength). However,
34 the performance of these elements in fire is not well known [4] and must be better understood
35 before they can be used with confidence in load-bearing applications where structural fire
36 resistance is required.

37 A limited number of fire resistance tests on fibre reinforced polymer (FRP) reinforced [5, 6,
38 7, 8, 9] or prestressed [10] concrete elements have been reported in the literature.
39 Unfortunately, however necessarily given the diversity of available FRP reinforcing or
40 prestressing products, each available study has used a specific FRP material, thus making it
41 difficult to draw general conclusions. Despite the scarcity of work studying the fire behaviour
42 of concrete structural elements incorporating FRP reinforcements, fundamental differences to
43 traditionally reinforced concrete structural elements have been reported [10]. Three important
44 failure mechanisms have been identified that may control the fire resistance (i.e. time-to-
45 failure in a standard fire resistance test) of reinforced or prestressed concrete elements,
46 namely:

- 47 1. heat-induced explosive concrete spalling;
- 48 2. thermo-mechanical bond degradation; and
- 49 3. thermo-mechanically induced longitudinal splitting cracks.

50 ***1.1 Heat-induced concrete spalling***

51 During (or even after) heating in fire, concrete at the exposed surface of structural elements
52 flakes away in a more or less violent manner. This phenomenon is known as ‘heat-induced
53 concrete spalling’ [11]. As a consequence, the concrete cover to the internal reinforcement

54 (steel or FRP) is reduced, resulting in rapid temperature increase of the reinforcement and
55 within the structural element, in addition to a direct influence on load bearing capacity due to
56 the loss of physical or effective cross sectional area.

57 Two main mechanisms are widely considered to contribute to the occurrence of heat-induced
58 concrete spalling. The first is a *thermo-hydraulic* mechanism associated with the transport
59 and/or evaporation of free water (or capillary water) within the concrete microstructure; this
60 is postulated to lead to generation of steam pressure and a ‘moisture clog’, and eventually to
61 spalling. It is almost universally agreed that higher moisture content results in increased heat-
62 induced spalling, all other factors being equal [12]. The second is a *thermo-mechanical*
63 mechanism associated with internal mechanical stresses resulting from through-thickness
64 temperature distributions and incompatibilities in the thermal and thermo-mechanical
65 behaviour of the components within the concrete matrix (e.g. coarse and fine aggregates,
66 cement paste, chemically bound water, etc). This mechanism can also be described at the
67 macro-scale, and linked to internal mechanical stresses resulting from external loading,
68 restraining forces, and/or differential thermal stresses arising due to uneven heating, through-
69 thickness temperature distributions, and/or the presence of cold areas.

70 The relative significance of these two mechanisms for a particular concrete mix, under a
71 particular thermal exposure in a given application, are not well known. Regardless of the
72 unquantified risk of spalling, current design and construction guidance for spalling prevention
73 (e.g. [13, 14]) is based on prescribing a dose of polypropylene (PP) fibres which is presumed
74 to assure limited spalling in applications with ‘relatively high’ spalling risk (e.g. high-
75 strength concrete, high in-service moisture content, high in-service compressive stress,
76 rapidly growing fires, etc). For example, European design guidelines for concrete in fire [13]
77 recommends including at least 2 kg of monofilament PP fibres per cubic metre concrete for

78 high-strength (>55 MPa cube compressive strength), high moisture content (>3% by mass)
79 and/or concrete with high inclusion of silica fume (>6% by mass of cement). Australian
80 design guidance for concrete in fire [14] states that the addition of 1.2 kg of 6 mm long
81 monofilament PP fibres per cubic metre concrete has a “dramatic effect in reducing the level
82 of spalling”.

83 **1.2 Thermo-mechanical bond degradation**

84 Reductions in bond strength between traditional steel reinforcement and concrete are not
85 generally considered to be a governing factor for the fire resistance of steel reinforced or
86 prestressed concrete elements [15]. Conversely, for FRP reinforcements it has been shown
87 that bond strength degradation between FRP tendons and concrete at elevated temperature
88 can be more critical than loss of FRP tensile strength [8, 16]. Thus, bond strength reduction is
89 widely considered a limiting factor for the fire safe structural design of FRP reinforced and/or
90 prestressed concrete elements [17]. The magnitude of bond strength reductions and their
91 impacts on the performance of FRP reinforced or prestressed concrete structures in fire
92 remain largely unknown, however, and have not been clearly demonstrated for many relevant
93 applications.

94 The bond between steel or FRP reinforcement (prestressed and/or non-prestressed) and
95 concrete deteriorates at elevated temperature [17, 18, 19, 20, 21]. These reductions are
96 reasonably well known for steel reinforcement and are given in available guidelines [13, 15];
97 however they remain largely unknown for virtually all currently available FRP
98 reinforcements [22, 23].

99 Design codes for the design of FRP reinforced or prestressed concrete structures typically
100 assume perfect bond between FRP reinforcement and concrete for ambient temperature

101 analysis and design (e.g. [24, 25, 26]). The bond strength of FRP reinforcements relies
102 primarily on the strength and stiffness of the epoxy resin at the surface of the reinforcement,
103 which normally incorporates a sand coating, spiral fibre roving, and/or a ribbed shaped resin.
104 However, the resin at the surface of the FRP tendon will soften at temperatures below 200°C
105 for most available products [4]; hence the assumption of perfect bond at elevated temperature
106 is not generally appropriate.

107 *1.3 Thermo-mechanically induced longitudinal splitting cracks*

108 FRP reinforcements exhibit vastly different coefficients of thermal expansion (CTEs) in their
109 longitudinal and transverse directions, and these also differ substantially from that of
110 concrete. For example, CFRP reinforcements tend to have lower (even negative) CTEs in the
111 longitudinal direction, while in the transverse direction their CTEs are governed by the matrix
112 polymer [24] and can be up to an order of magnitude larger than for concrete [27]. CTE for
113 FRPs is traditionally examined in the range of temperatures before decomposition of the
114 matrix polymer; 300-350°C [4, 27].

115 Prior studies have aimed at understanding the effects of differential thermal expansion
116 between FRP reinforcements and concrete [27, 28, 29, 30, 31]. Presently, it is thought that the
117 development of splitting stresses within the concrete cover leads to the development of heat-
118 induced longitudinal (reflective) splitting cracks along the reinforcement, and possibly to loss
119 of the concrete cover's ability to provide sufficient confining action for anchorage to be
120 maintained. It is expected that this may be exacerbated by extreme through-thickness
121 temperature distributions in the concrete during fire [10].

122

123 2 RESEARCH SIGNIFICANCE

124 It is widely perceived that reinforced or prestressed concrete structural elements
125 incorporating FRP reinforcements have lower fire resistance than equivalent steel reinforced
126 or prestressed elements [10]. However, comparatively few large-scale fire resistance tests (or
127 structural fire tests) have been performed on FRP reinforced or prestressed concrete elements;
128 little is known about the ‘true’ response of these elements during standard fire resistance tests
129 in furnaces. The current paper aims to understand the relative importance of the foregoing
130 issues on fire resistance of FRP prestressed concrete elements using standard fire testing.

131 3 EXPERIMENTAL PROGRAM

132 Five large-scale, loaded CFRP prestressed HPSCC slabs were tested simultaneously in a
133 single standard floor furnace test [32]. The design of the slabs was aimed to evaluate the
134 influence of concrete mix and PP fibre dose (spalling), overall slab depth (tendons
135 temperature), and the presence of CFRP grids within the anchorage zones (splitting cracking
136 in the anchorage zones) (see Table 1).

137 **Table 1 – Evaluated parameters, time-to-failure and failure mechanisms for slabs discussed herein.**

Slab #	Concrete mix	Depth of the slab [mm]	CFRP grids	Applied load per point [kg]	Slab utilization factor	CFRP utilization factor	Time-to-failure [mm' ss'']	Failure mechanism
1	A	45	No	25.0	0.23	0.42	42' 01"	Loss of anchorage
2	A	45	Yes	25.0	0.23	0.42	12' 37"	Explosive spalling
3	A	60	Yes	38.4	0.20	0.43	22' 10"	Explosive spalling
4	B	45	Yes	25.0	0.23	0.42	50' 27"	Loss of anchorage
5	B	60	Yes	38.4	0.20	0.43	93' 04"	Loss of anchorage

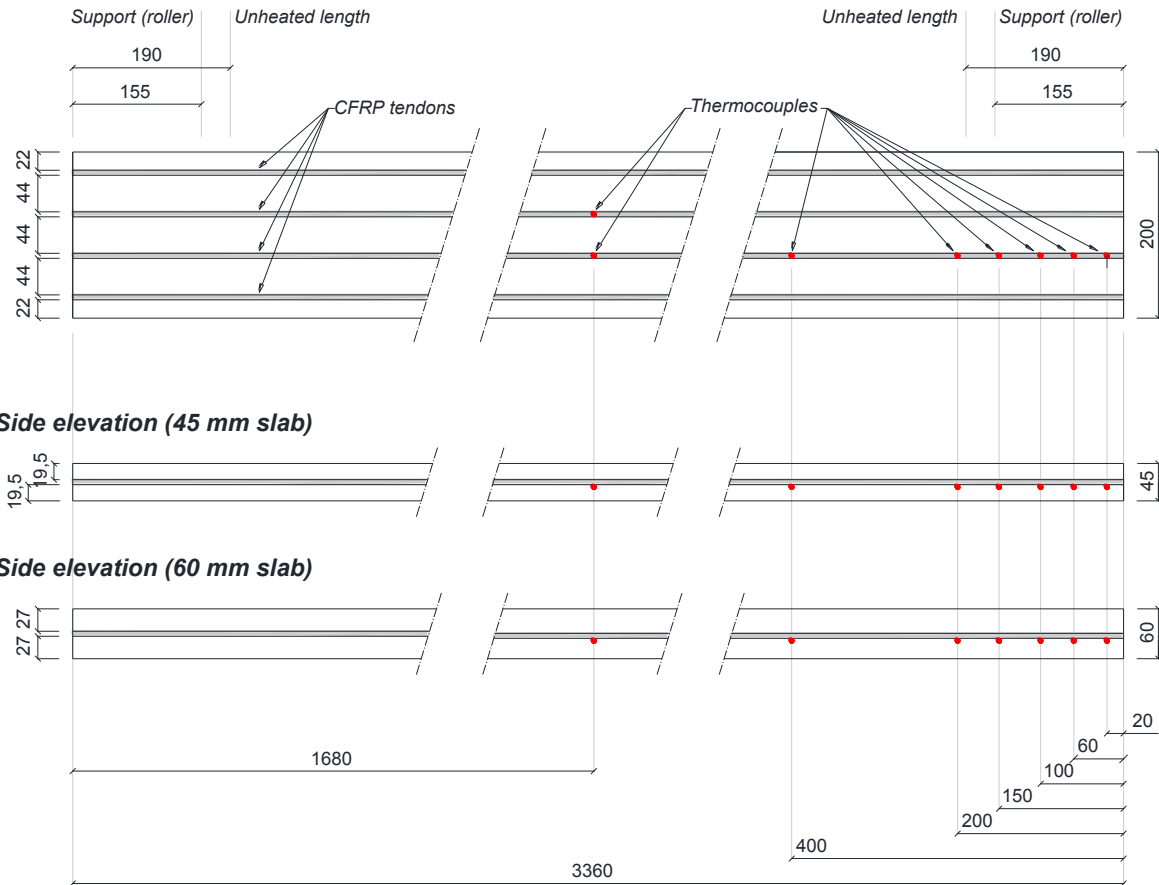
138 **3.1 Test specimens**

139 The tested slabs were similar to those used by the authors in prior research [10]. Their overall
140 length was 3360 mm (see Figure 2) and they were prestressed with four circular pultruded,
141 quartz sand-coated CFRP tendons stressed to an initial prestress level of 1,000 MPa. Initial
142 prestress level was calculated based on the gross cross-sectional area of the tendons; i.e
143 without considering the layer of sand coating (refer to Section 3.2.2 of this paper). It is
144 noteworthy to point out that for prestressed concrete elements, the ends the slabs are
145 commonly labelled as active end (stressing end) and passive end (dead end).

146 All CFRP tendons were located at the slab mid-depth, with a tolerance of ± 2 mm, to obtain a
147 nominally concentric prestressing force (see Figure 3). The slabs were 45 or 60 mm thick
148 (refer to Table 1), leading to clear concrete covers to the prestressed CFRP reinforcement of
149 19.5 mm and 27 mm, respectively. All slabs were 200 mm wide. Lateral clear concrete cover
150 at the slab edges was 22 mm in all cases, with a tendon-to-tendon clear spacing of 44 mm
151 (see Figure 3).

152

Plan view

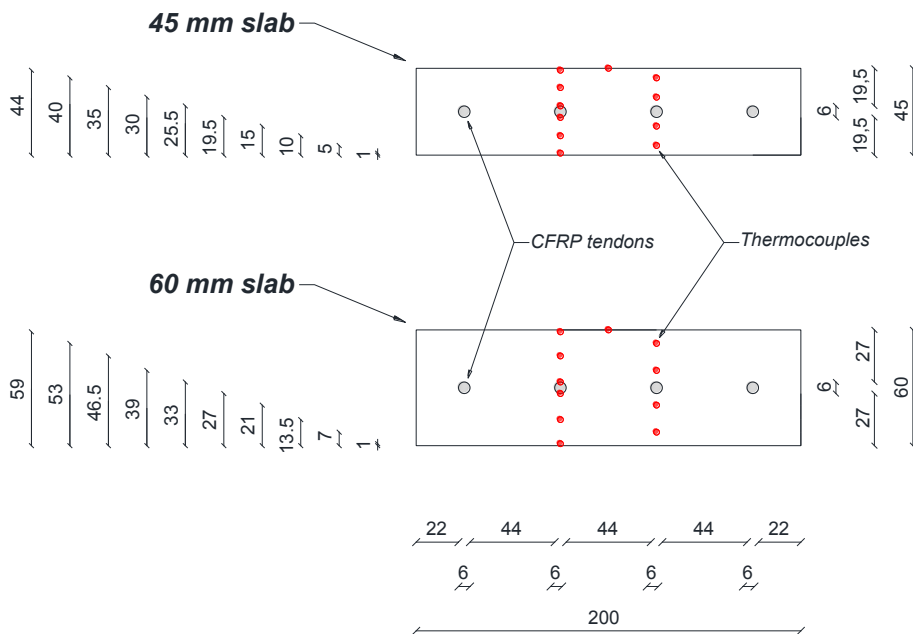


153

154

155

Figure 2 –Plan view and side elevations for slabs 45 and 60 mm thick, also showing thermocouples position (CFRP grids in the anchorage zones are not shown).



156

157

Figure 3 – Cross section for slabs 45 and 60 mm thick, also showing thermocouples position.

158 **3.2 Constituent materials**

159 **3.2.1 High-Performance, Self-Consolidating Concrete (HPSCC)**

160 All slabs were fabricated from a high-performance, self-consolidating concrete (HPSCC) of
 161 strength class C90 (minimum 28 day 150 mm cube compressive strength of 90 MPa). Given
 162 the high likelihood of spalling for this mix due to its high strength and the inclusion of
 163 microsilica in the mix [13], 2.0 kg of 3 mm long or 1.2 kg of 6 mm long PP monofilament
 164 fibres (32 µm in diameter) were included for mixes A and B, respectively. Detailed of both
 165 mixes are given in Table 2.

166 Moisture content was measured by dehydration mass loss of control specimens. The average
 167 moisture contents at the time of testing were 3.6 and 3.9% by mass, for mixes A and B,
 168 respectively. Compressive and splitting tensile strengths [33] were measured at 28 days and 6
 169 months (close to the time of testing), and are given in Table 2.

170 of testing), and are given in Table 2.

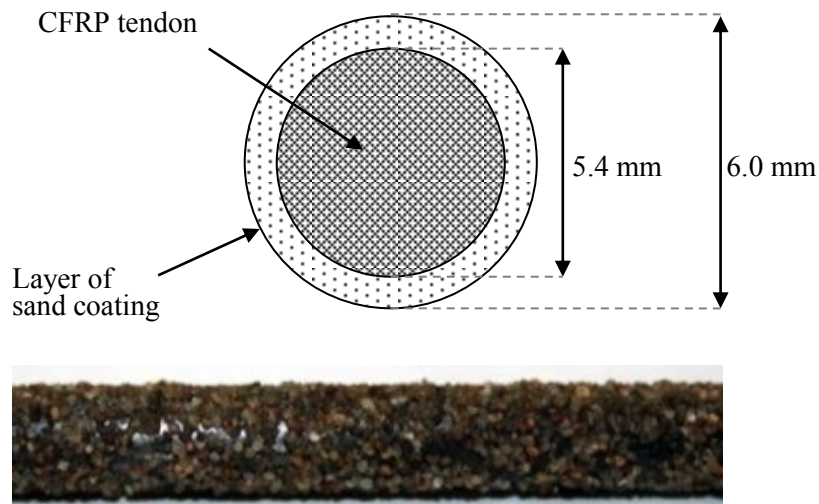
171 **Table 2 – Mix composition and slump flow for the HPSCC mixes.**

		Mix #A	Mix #B
Water/(cement + microsilica + fly ash)	[-]	0.31	0.31
Cement (includes 20% microsilica)	[kg/m ³]	475	469
Fly ash	[kg/m ³]	120	120
Limestone aggregate (0-8 mm)	[kg/m ³]	1675	1669
Superplasticizer in % of cement	[%]	1.69%	1.75%
Polypropylene fibres	[kg/m ³]	2.0 (3 mm PPs)	1.2 (6 mm PPs)
Slump flow [34]	[mm]	830	785
Compressive strength (28 days / 6 months)	[MPa]	92.6 / 93.3	96.2 / 98.5
Splitting tensile strength (28 days / 6 months)	[MPa]	5.44 / 5.47	5.49 / 5.57
Moisture content (at the time of testing)	[% by mass]	3.6%	3.9%

172

173 3.2.2 CFRP prestressing tendons

174 The pultruded uniaxial CFRP tendons used herein were made from Tenax UTS carbon fibres,
175 at a fibre volume fraction of 64%, and Bakelite 4434 epoxy resin. Their design tensile
176 strength was 2,000 MPa, with a design elastic modulus of 150 GPa [35] and a characteristic
177 ultimate strain of 1.33%. The quartz sand coating applied after the initial pultrusion process
178 had an average grain size of 0.5 mm and was bonded using the same epoxy resin to promote a
179 strong bond. The gross (or net) diameter of the CFRP tendons was 5.4 mm and the total
180 diameter, including sand coating, was approximately 6.0 mm (see Figure 4).



181

182 **Figure 4 – Cross section schematic and photo of the CFRP prestressing tendon used in the current study.**

183 3.2.3 CFRP grid reinforcement

184 In an attempt to limit splitting cracking and improve the bond strength in the prestress
185 anchorage zones at elevated temperatures, commercially available CFRP grids (C-GRID®)
186 were placed locally within the anchorage zones of four of the five slabs (refer to Table 1).
187 Prior to casting, these CFRP grids were placed above and below the CFRP tendons (see
188 Figure 5). The aim was to minimize heat-induced longitudinal splitting cracks, and hence loss
189 of confining action provided by concrete in the anchorage zones. The CFRP grids had

190 transverse and longitudinal spacings of 46 mm and 41 mm, respectively, with a design tensile
191 elastic modulus of approximately 120 GPa in both directions.

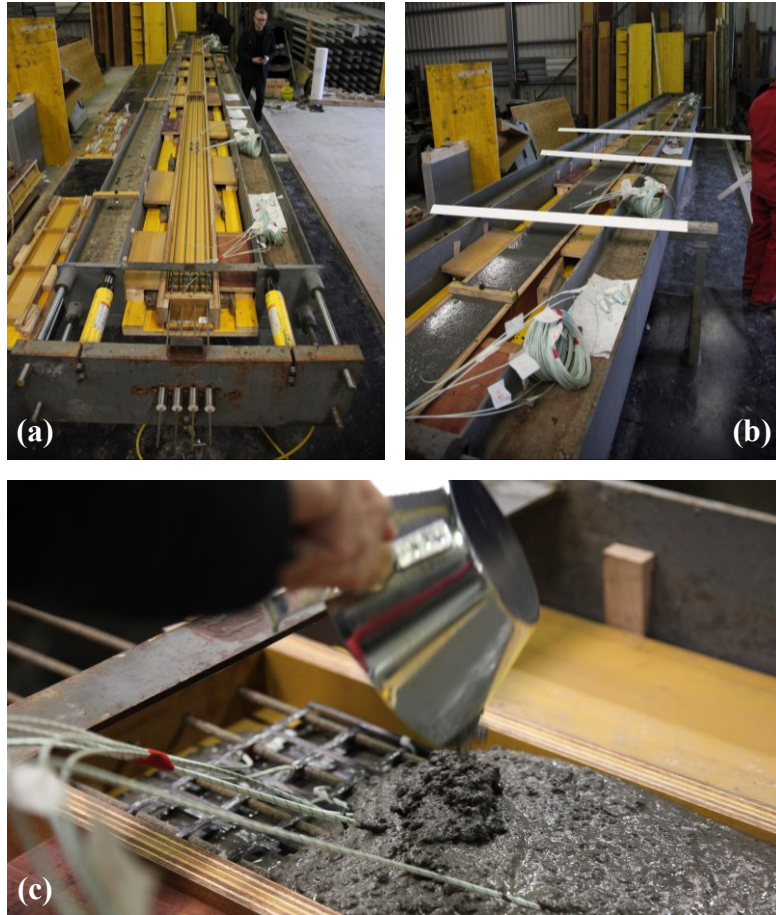


192
193 **Figure 5 – Placement of CFRP grids within the anchorage zones (above and below the CFRP tendons).**

194 **3.3 Casting and curing procedures**

195 The formwork (i.e. prestressing bed) allowed for simultaneous casting of three prestressed
196 slabs at one time (see Figure 6). The mixing and casting procedure was performed according
197 the exacting standards for typical precast concrete elements fabricated by the industrial
198 partner (a Swiss precast company). After casting, slabs were covered with polyethylene
199 sheeting for 72 hours before the prestress was transferred and the forms stripped. The slabs
200 were cured in a moist condition under polyethylene sheets for a further five days, and were
201 then left to cure under ambient conditions for 1.5 months in the production hall of the precast
202 company before being delivered to the Empa Fire Testing Laboratory where they were stored
203 indoors until testing. Slabs were tested at an age of 5.2 months (testing authorities typically
204 prescribe a minimum age of 3 months for furnace testing of concrete [32]). Cube and cylinder
205 specimens were also cast to determine compressive and splitting tensile strength, as well as
206 average moisture content at the time of testing.

207



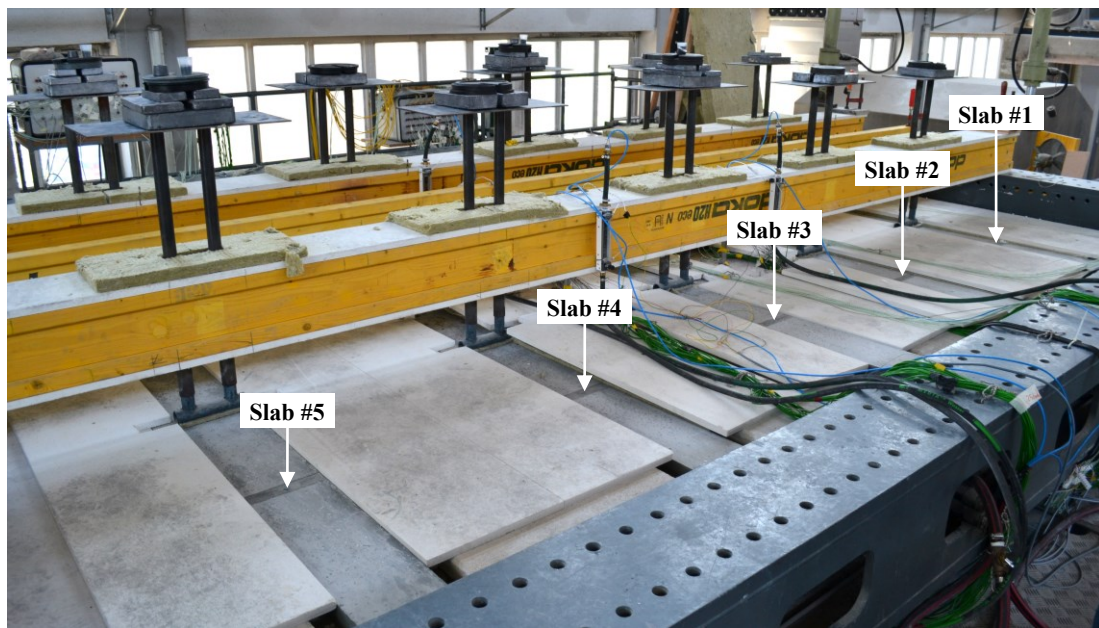
208

209 **Figure 6 – Photographic sequence showing (a) prestressing bed and formwork prior to casting, (b) casting**
210 **procedure of large-scale specimens, and (c) close-up during casting of the anchorage zone (with CFRP**
211 **grids and thermocouples).**

212

213 **4 LARGE-SCALE FURNACE TEST**

214 A large-scale furnace test (standard fire resistance test) was performed at Empa's Fire Testing
215 Laboratory in Dübendorf, Switzerland. The five specimens described previously were
216 simultaneously loaded and exposed to a standard fire (see Figure 7) using a floor furnace
217 [32].



218

219 **Figure 7 – Photo of the fire resistance test setup showing positions of the respective slabs and sustained**
220 **loading technique used.**

221

222 4.1 Test setup

223 The test was performed in accordance to the European requirements of the standard fire
224 resistance test [32].

225 4.1.1 Thermal loading

226 The setup of the specimens was aimed at assuring one-sided heating from below, so the sides
227 of the specimens were fully insulated. The heating regime was executed according to the
228 requirements of the standard time-temperature curve [32]. Since no clear influence of an
229 unheated anchorage length in excess of 160 mm had been observed during a prior series of
230 furnace tests performed by the authors [10], it was decided to maintain a constant but
231 conservative (and essentially arbitrary) unheated anchorage length of 195 mm for all five
232 specimens (refer to Figure 2). Thus, the overall exposed length of the 3360 mm long slabs
233 was 2970 mm.

234 4.1.2 Mechanical loading

235 Sustained mechanical loading was applied to simulate an in-service condition for the slabs, in
236 simply-supported four-point bending. End supports (rollers) were placed 155 mm from the
237 slabs' ends, leading to a structural span of 3050 mm (see figures 8 and 9). The applied load
238 was designed to be sufficient to achieve decompression at the extreme tension fibre within
239 the constant moment region (i.e. $\sigma_{c,bottom} = 0$ [MPa]); this corresponds to a typical design service
240 load condition for a façade element of this type in a real building [1]. Loading was imposed
241 30 minutes prior to start of heating.

242 Prestressing losses due to elastic shortening, shrinkage and creep of the concrete were
 243 considered and calculated based on results from prior experimental studies performed for
 244 similar HPSCC mixes [36]. Total prestressing losses ($\Delta\sigma_p^{Total}$) were calculated as:

$$245 \quad \Delta\sigma_p^{Total} = \Delta\sigma_p^{ES} + \Delta\sigma_p^{SR} + \Delta\sigma_p^{CR} \quad (1)$$

246 Losses due to elastic shortening of concrete were calculated as:

$$247 \quad \Delta\sigma_p^{ES} = \frac{E_{CFRP}}{E_c} \cdot \sigma_{c,0} \quad (2)$$

248 where:

$$249 \quad \sigma_{c,0} = \sigma_{CFRP,0} \cdot \frac{A_{CFRP}}{A_c - A_{CFRP}} \quad (3)$$

$$250 \quad E_c = 32.5 \text{ [GPa]} \quad (\text{at 2-3 days}) \text{ [36]} \quad (4)$$

$$251 \quad E_{CFRP} = 150 \text{ [GPa]} \quad [35] \quad (5)$$

252 Losses due to shrinkage of concrete were calculated as:

$$253 \quad \Delta\sigma_p^{SR} = E_{CFRP} \cdot (-\varepsilon_c^{SR}) \quad (6)$$

254 Concrete strains due to shrinkage (ε_c^{SR}) at the time of testing were calculated by interpolating
 255 between measurements on HPSCC control specimens at various ages [36]. Losses due to
 256 creep of concrete were calculated as:

$$257 \quad \Delta\sigma_p^{CR} = \varphi_c \cdot \frac{E_{CFRP}}{E_c} \cdot \sigma_{c,creep} \quad (7)$$

258 where:

$$\sigma_{c,creep} = \varphi_{CFRP} \cdot \left(\sigma_{CFRP,0} \cdot \frac{A_{CFRP}}{A_c - A_{CFRP}} \right) \quad (8)$$

The concrete creep coefficient (φ_c) and bond creep coefficient (φ_{CFRP}) were defined based on results from prior experimental studies performed for similar specimens [36].

Finally, initial prestressing level at the time of testing were calculated as:

$$\sigma_{CFRP,rest} = \sigma_{CFRP,0} - \Delta\sigma_p^{Total} \quad (9)$$

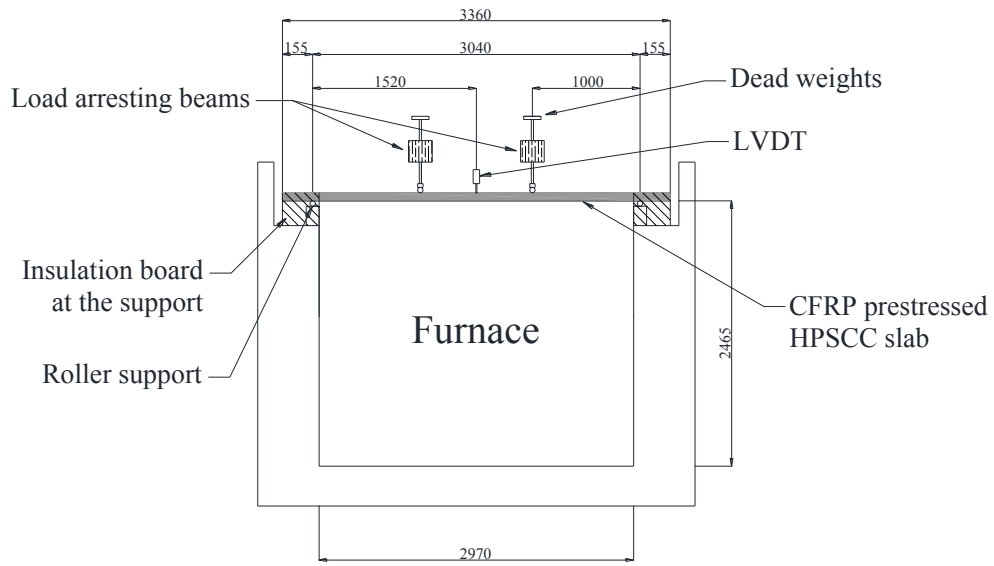
and prestress losses could then be calculated as:

$$\text{Prestressing losses (\%)} = \frac{\Delta\sigma_p^{Total}}{\sigma_{CFRP,0}} \times 100 \quad (10)$$

Prestressing losses for 5.2 month old slabs with CFRP tendons initially prestressed to 1,000 MPa were calculated as 16% and 14% for the 45 and 60 mm thick slabs, respectively (refer to Table 1). The slab utilization factors, calculated as the ratio between the applied mechanical load during testing and the theoretical ultimate failure load at ambient temperature, assuming concrete crushing at the compressive zone [11], were 0.23 and 0.20 for the 45 and 60 mm thick slabs, respectively.

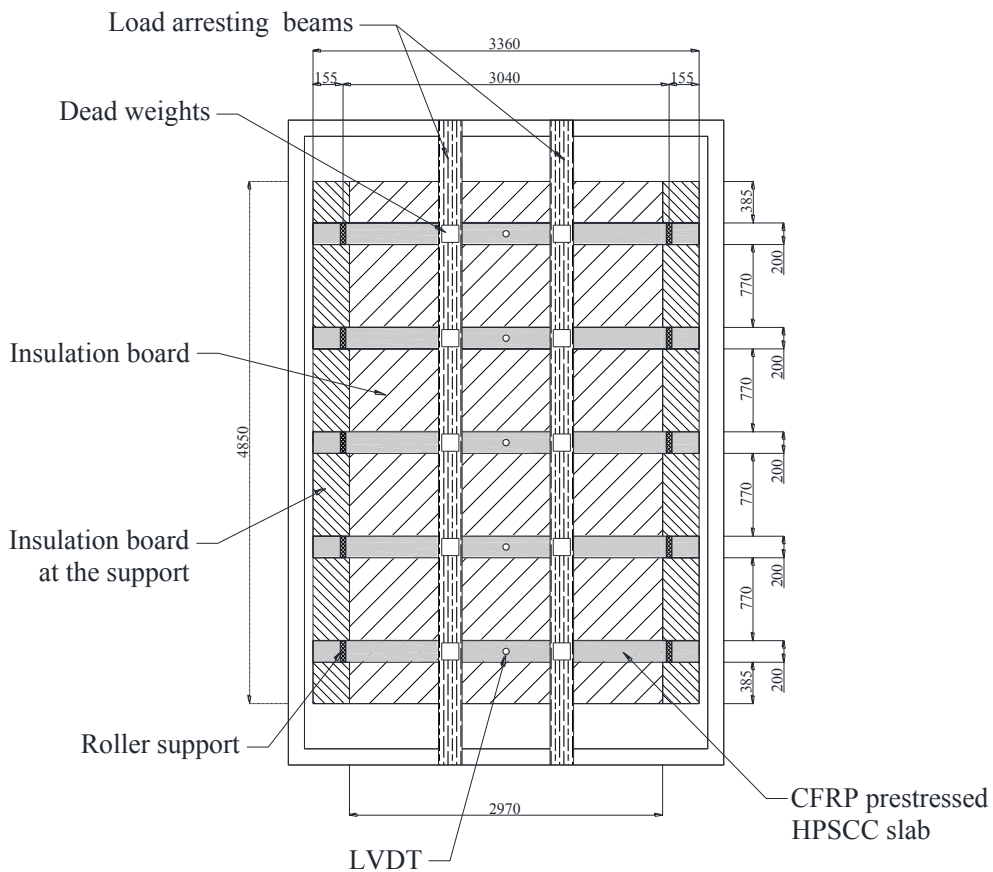
The CFRP utilization factor was calculated as the ratio between the initial strain of the CFRP tendons during testing (considering losses) and their characteristic ultimate failure strain. Before heating these were 42 and 43% of the CFRPs' design tensile strength capacity for the 45 and 60 mm thick slabs, respectively.

276



277

278 **Figure 8 – Test setup, loading, and selected instrumentation for the fire resistance test (side elevation).**



279

280 **Figure 9 – Layout of test specimens during the fire resistance test (plan view).**

281 4.2 Instrumentation

- 282 • *Furnace temperature gauges* – In accordance with fire test standards [32] eight standard
283 plate thermometers were positioned inside the furnace. These were used to record and
284 control the temperatures inside the furnace during testing.

- 285 • *Temperature gauges inside the slabs* – Through-thickness temperature measurements
286 were taken at midspan at eleven distances from the exposed surface of each of the slabs
287 (see Figure 3). Temperature measurements were also taken at several locations in the
288 anchorage zones (active end only) along the lower edge of one central CFRP tendon (see
289 Figure 2). Bare K-type thermocouples (TCs) were used in all cases, and special care was
290 taken during the casting process to ensure precise placement of the TCs at the intended
291 location inside the slabs.

- 292 • *Midspan vertical displacement gauges* – Midspan vertical deflection was measured using
293 linear voltage displacement string pot transducers, placed on a beam resting on top of the
294 furnace.

- 295 • *Draw-in gauges* – Aiming to measure possible draw-in of the CFRP tendons during
296 testing due to loss of anchorage from heating or splitting cracking of the anchorage zones
297 high accuracy yet economical, semi-disposable custom-built “pi” displacement gauges
298 (pi-gauges) were designed and fabricated for the project described herein (one of these
299 gauges is shown in Figure 10). These were placed at either end of the slabs (active and
300 passive ends). These ‘pi-gauges’ consisted of foil strain gauges applied to a piece of
301 curved spring steel, which when flexed due to deformation could be correlated to
302 displacement. To obtain the required accuracy of the instruments, the gauges were
303 designed with a half-bridge connection with strain gauges placed on the top and bottom

304 of each pi-gauge (see Figure 10). The pi-gauges were calibrated over a displacement
305 range of ± 4 mm. Draw-in measurements were performed for all four CFRP tendons, at
306 both ends of slabs #1, #2, and #3 (refer to Table 1).



307
308 **Figure 10 – Custom-fabricated ‘pi-gauges’ (left) and gauges installed for measuring tendon draw-in for**
309 **all four tendons at one end of Slab #1 (right).**

310 **5 TEST RESULTS AND ANALYSIS**

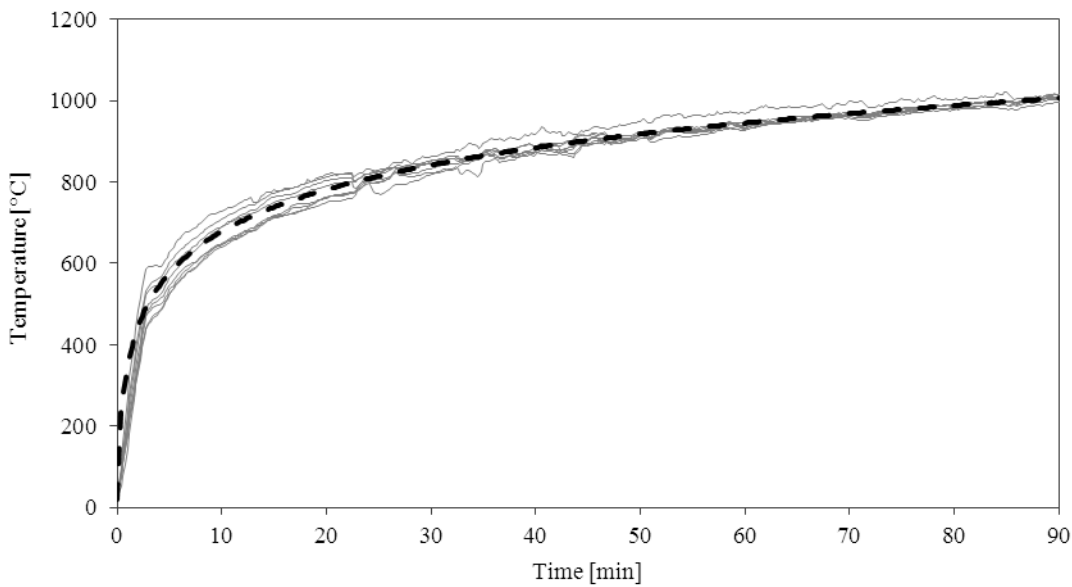
311 The observed time-to-failure of all five test specimens is shown in Table 1, along with their
312 respective failure modes. Failure was driven by either:

- 313 • a single explosive heat-induced spalling event, which resulted in immediate and total
314 collapse of the test specimen (slabs #2 and #3); or
- 315 • progressive loss of bond between the tendon and the concrete in the anchorage zone,
316 leading to more gradual collapse of the test specimen (slabs #1, #4, and #5).

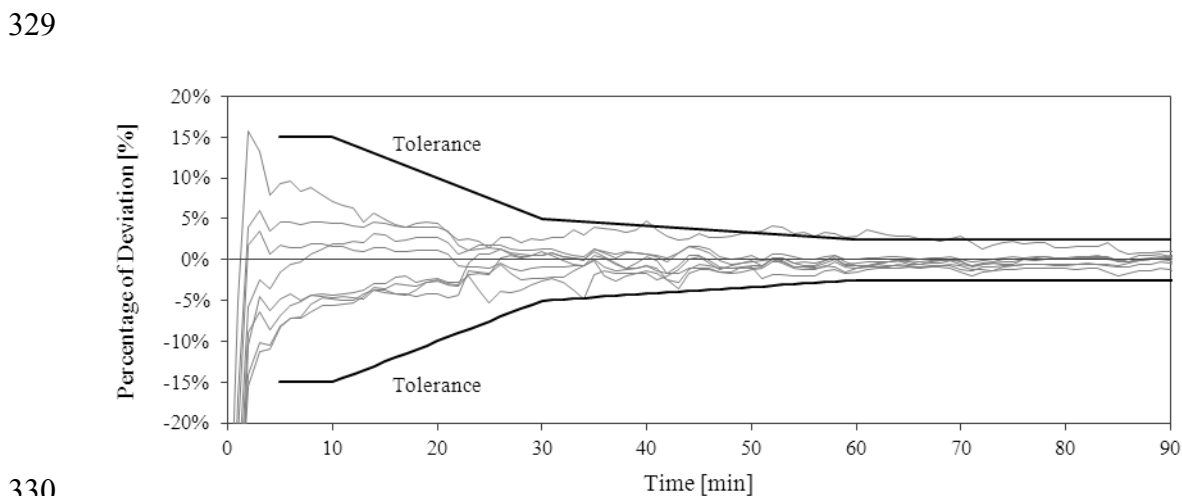
317 **5.1 Furnace temperature**

318 Temperature measurements from the eight plate thermometers inside the furnace are shown
319 in Figure 11 along with the objective time-temperature curve. Although compliant with the

320 testing standard [32], the temperature measurements show substantial deviation in the
321 temperature measured inside the furnace, especially during the first 20 minutes (see Figure
322 12). Due to the obvious technical challenge of precisely controlling the furnace to follow the
323 rapidly growing prescribed time-temperature curve [32] during early stages of the test, most
324 testing standards do not prescribe an allowable deviation during the first 5 minutes (see
325 Figure 12).



326
327 **Figure 11 – Furnace gas temperatures measured by the plate thermometers along with the objective**
328 **standard time-temperature curve [32].**

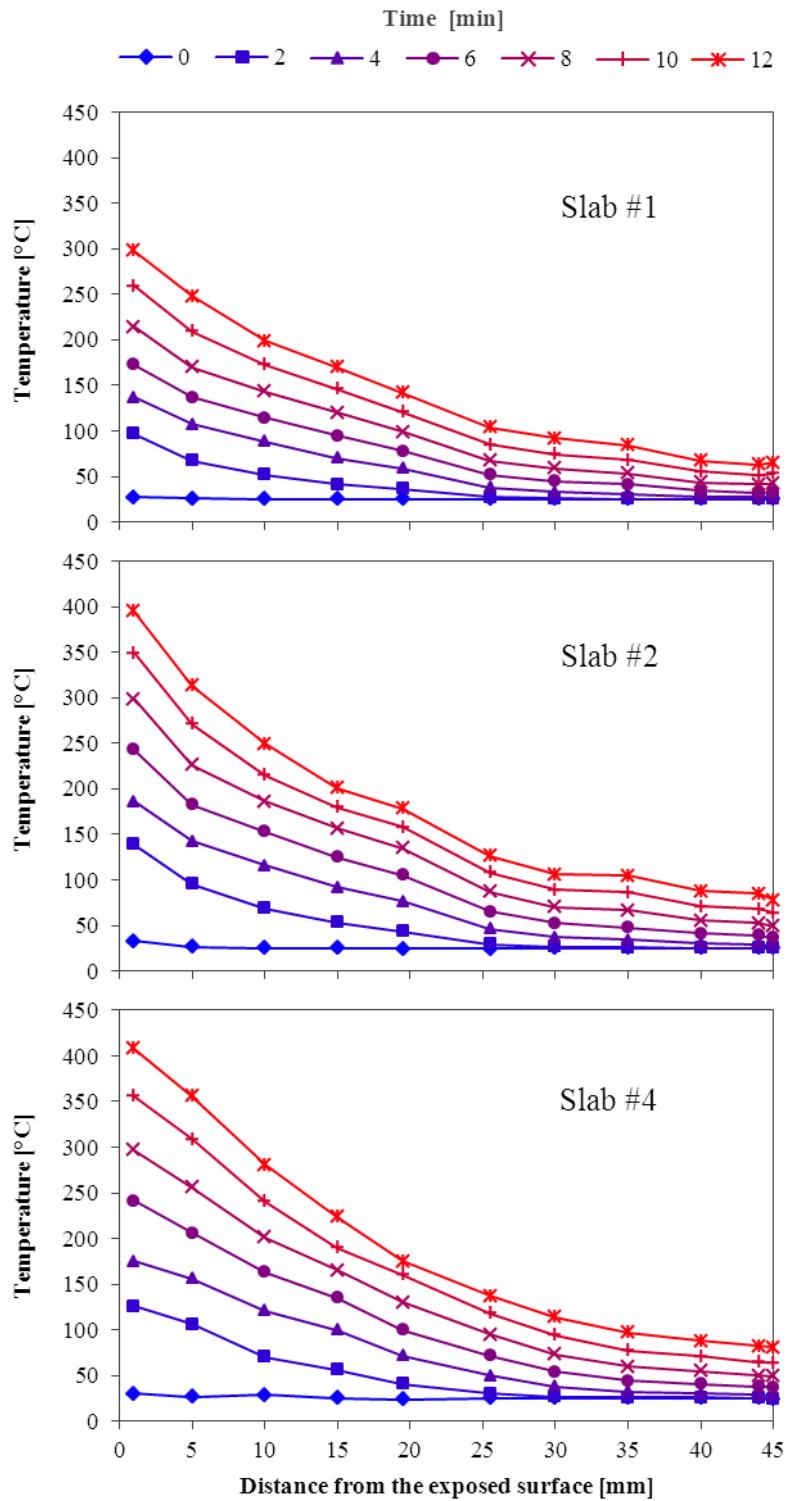


330
331 **Figure 12 – Percentage of deviation of the temperature measured by plate thermometers from that of the**
332 **objective temperature, and the maximum allowable deviation (tolerance) [32].**

333 **5.2 *Through-thickness temperatures at midspan***

334 A comparison of through-thickness temperature distributions measured at midspan is shown
335 in figures 13 and 14 for slabs 45 and 60 mm thick, respectively. Temperature for the first 12
336 minutes of the test are shown; the time at which the first of the slabs failed due to explosive
337 spalling (refer to Table 1).

338 Considerable variation of through-thickness temperature distributions was observed for slabs
339 with equivalent thickness, possibly demonstrating poor homogeneity of the thermal
340 exposures for slabs tested simultaneously during a single furnace test; this is despite the
341 temperatures measured by the plate thermometers complying with the test standard. Figure 13
342 suggests a more rapid through-thickness temperature increase for 45 mm thick slabs
343 positioned near the centre of the furnace, slabs #2 and #4, relative to Slab #1 positioned near
344 the edge of the furnace (see Figure 7). A similar, however less severe, comparison is shown
345 in Figure 14 for Slab #3, positioned at the centre of the furnace, and Slab #5, positioned near
346 the edge of the furnace.



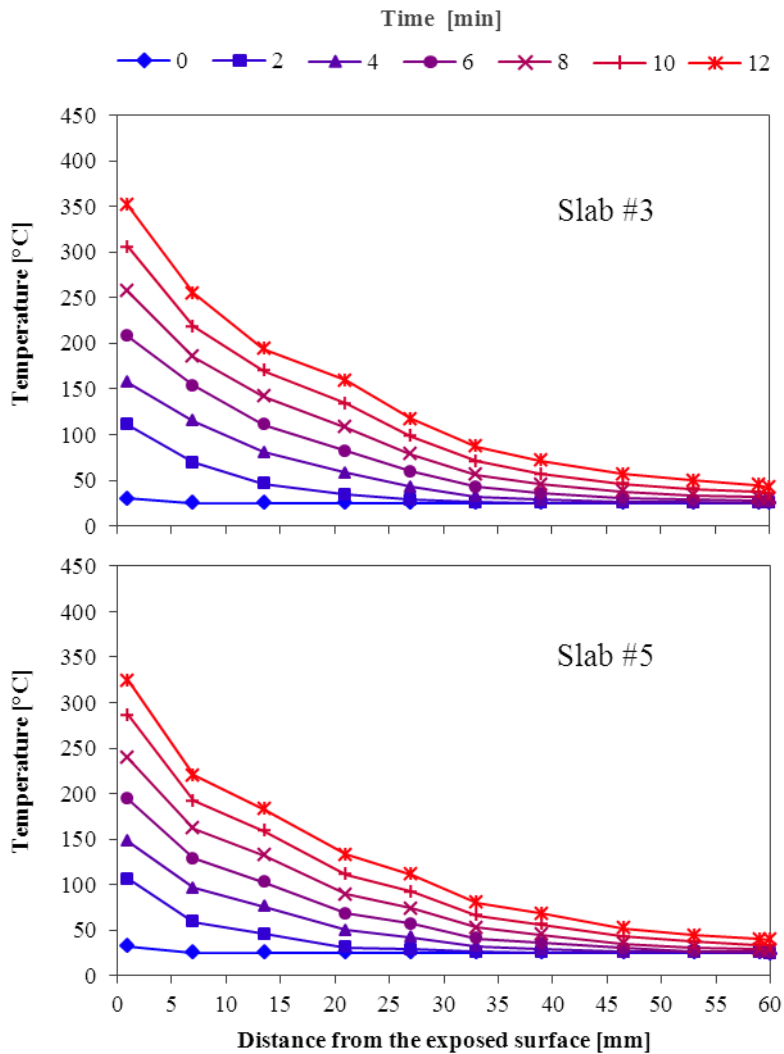
347

348

Figure 13 – Midspan through-thickness temperature distributions for 45 mm thick slabs at 2 minute intervals during the first 12 minutes of the furnace test.

349

350



351
 352 **Figure 14 – Midspan through-thickness temperature distributions for 60 mm thick slabs at 2 minute**
 353 **intervals during the first 12 minutes of the furnace test.**

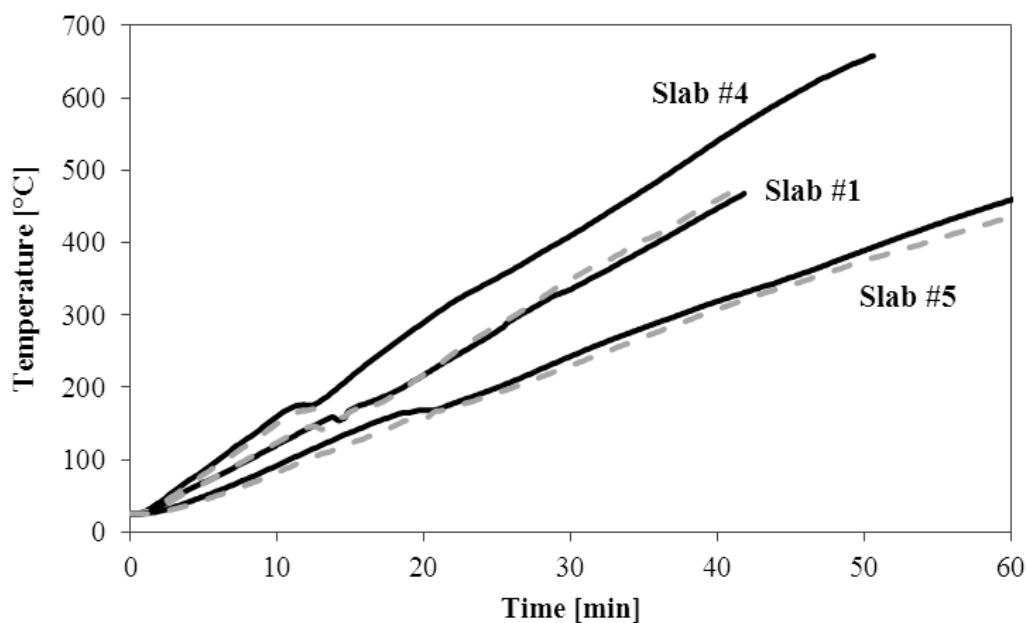
354 **5.3 Temperature in the anchorage zone**

355 Figure 15 shows a comparison of the temperature of the CFRP tendon at midspan and at 400
 356 mm from the end of the slab (still within the heat exposed zone of the slab, see Figure 2) for
 357 slabs #1, #4, and #5 (all of which failed due to loss of anchorage). Figure 15 suggests that the
 358 temperature of the CFRP tendons was essentially constant over the exposed length of the
 359 slabs. It is noteworthy that thermocouples were placed along the lower edge of an interior
 360 CFRP tendon, and therefore recorded the temperature at the interface between the tendon and
 361 the concrete, rather than the temperature of the CFRP itself. Due to the low thermal inertia of

362 the CFRP tendons relative to that of concrete, the temperature inside the tendon may be lower
363 than that at the tendon-concrete interface in the fire exposed zone (e.g. at midspan); while the
364 opposite may be true in the unheated overhangs.

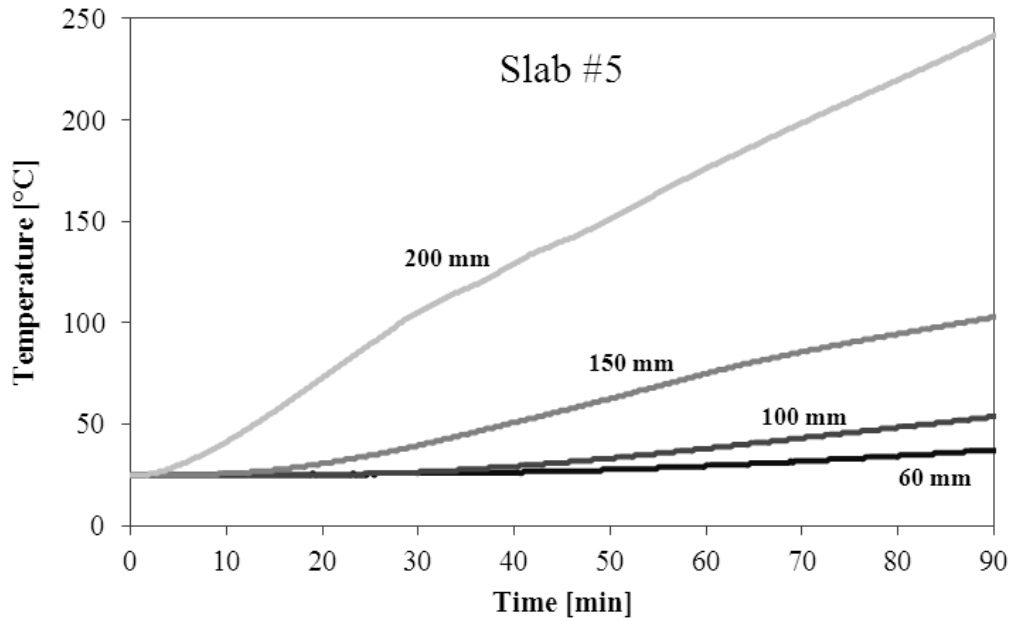
365 Figure 16 shows a comparison of the temperatures measured in the anchorage zone for Slab
366 #5, demonstrating the effectiveness of maintaining a ‘cool’ anchorage zone when designing
367 for unheated overhangs.

368 Within the scope of the work presented herein, no attempt was made to individually identify
369 the relevance of the two potential mechanisms for loss of anchorage: thermo-mechanical
370 bond degradation in the anchorage zone and/or thermo-mechanically induced longitudinal
371 splitting cracking. Further work is needed to better understand the drivers for, and
372 consequences of, both mechanisms.



373

374 **Figure 15 – Comparison between temperatures of the CFRP tendons measured at midspan (continuous**
375 **line) and at 400 mm from the end of the slab (segmented line) for slabs #1, #4, and #5.**

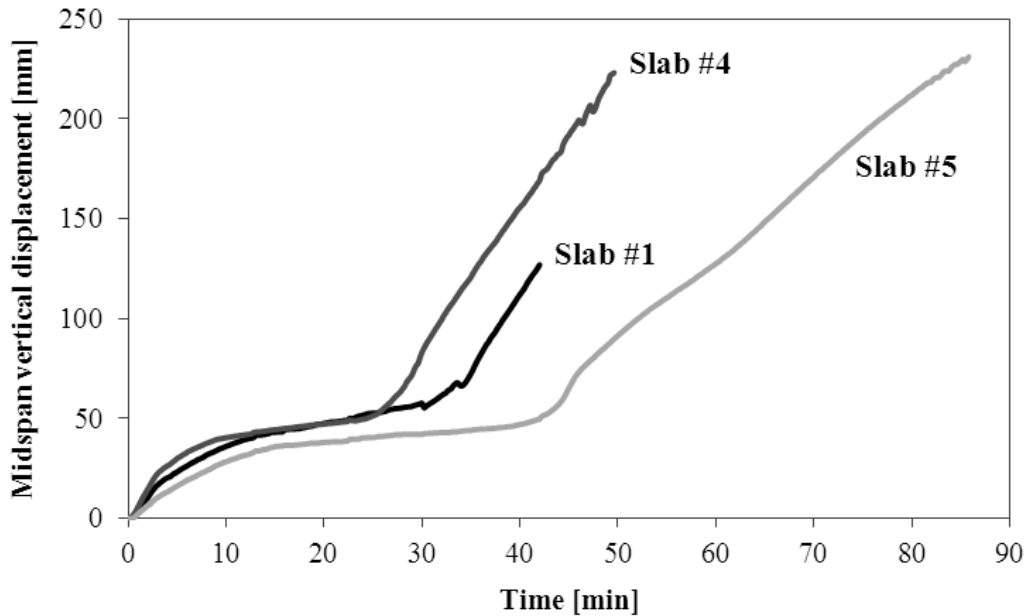


376

377 **Figure 16 – Typical temperature within the unheated overhang for a central CFRP tendon (Slab #5, 60**
 378 **mm thick), for distances of 60, 100, 150, and 200 mm from the end of the slab.**

379 **5.4 Midspan vertical displacement**

380 Figure 17 shows the time-history of midspan vertical displacements for the slabs that failed
 381 due to loss of anchorage. During the early stages of the test, midspan deflections were
 382 induced predominantly by thermal bowing. During this stage an obvious influence of the
 383 slabs' thickness was observed [37]; wherein thicker slabs experienced less vertical midspan
 384 deflection due to lower thermally induced curvatures. Comparison of midspan deflections for
 385 slabs #1 and #4 (both 45 mm thick), during the first 10 minutes of the tests, shows that the
 386 more rapid increases of through-thickness temperature (observed for slab #4, refer to Figure
 387 13) resulted in a more rapid increase in midspan deflection due to thermal bowing (see Figure
 388 17). For slabs #1, #4, and #5, all of which failed due to loss of anchorage, a clear change of
 389 slope in the time-history of midspan deflections, presumed to be associated with loss of
 390 anchorage, was observed (discussed later).

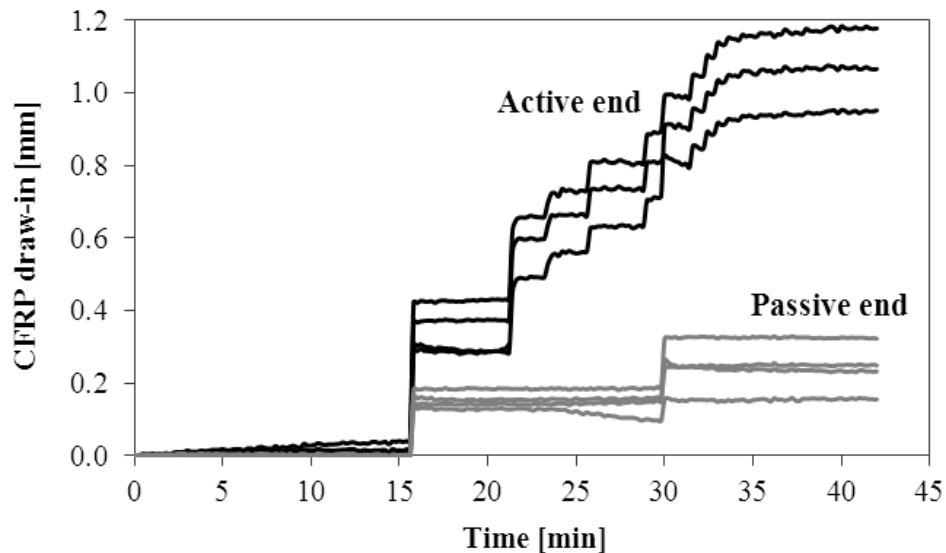


391

392 **Figure 17 – Time-history of midspan vertical displacement measurements for all slabs that failed due to**
 393 **loss of anchorage (slabs #1, #4, and #5).**

394 **5.5 Draw-in of CFRP tendons**

395 Draw-in measurements were taken for all four CFRP tendons at both ends of slabs #1, #2,
 396 and #3. Unfortunately, because slabs #2 and #3 failed catastrophically at an early stage of the
 397 test due to explosive concrete spalling, no useful draw-in measurements were recorded for
 398 these slabs. For Slab #1 however, tendon draw-in measurements were taken until failure, at
 399 42 minutes from the start of the test as shown in Figure 18. While no attempt was made to
 400 quantify the relationship between draw-in measurements and the failure mechanism of Slab
 401 #1, a qualitative analysis considering draw-in measurements, loss of anchorage, and failure is
 402 presented later.



403

404 **Figure 18 – Draw-in measurements for tendons at the active and passive ends of Slab #1 during testing.**

405 **6 ANALYSIS AND DISCUSSION**

406 **6.1 Failure due to spalling**

407 Failure of slabs #2 and #3 was driven by the occurrence of single explosive concrete spalling
 408 events, 12 and 22 minutes from the start of the test, respectively (refer to Table 1).
 409 Immediately after spalling, each of these slabs suffered catastrophic failure and collapsed into
 410 the furnace. Video stills recorded during testing showed the moment at which spalling
 411 occurred (shown for Slab #2 in Figure 19).

412 Slab #2 failed after 12 minutes, whereas the virtually identical Slab #1 failed due to loss of
 413 anchorage after 42 minutes of fire exposure (refer to Table 1); Figure 13 shows that Slab #2
 414 experienced more rapid heating during the early stages of the test. This suggests a possible
 415 important influence of the time-history of through-thickness temperatures on the occurrence
 416 of heat-induced concrete spalling [11]. For instance, Slab #2 spalled when the measured
 417 temperature 1 mm from its exposed surface was 400°C, while for Slab #1 the temperature at
 418 the same location was only 300°C. The possibility that this was due to misplacement of

419 thermocouples during casting was discarded since equivalent temperature differences
420 between slabs #1 and #2 were observed for temperatures measured at various positions in the
421 slab (e.g. 5, 10, and 15 mm from the exposed surface).

422 For slabs #4 and #5, both of which were cast from Mix B, no spalling was observed and thus
423 it is not possible to determine whether time-history of through-thickness temperatures might
424 influence the occurrence of spalling for this mix. The above demonstrates an inability to
425 properly compare test results for multiple specimens simultaneously tested during a single
426 furnace test when subtle differences in thermal gradients play important roles in the test
427 outcomes.



428

429

Figure 19 – Explosive spalling and immediate collapse of Slab #2 at 12' 37".

430 6.2 Failure due to loss of anchorage

431 The failure mechanism for slabs #1, #4, and #5 was driven by loss anchorage of the CFRP
432 tendons, which resulted in structural failure at 42, 50, or 93 minutes from the start of the test,
433 respectively (refer to Table 1). As already noted, loss of anchorage for high-performance
434 CFRP prestressed concrete structural elements during fire resistance tests has previously been
435 postulated to be driven by a combination of thermo-mechanical bond degradation, thermo-
436 mechanically induced longitudinal splitting cracks, or a combination of both mechanisms.

437 Identifying (either experimentally or theoretically) the relative influences of these factors is
438 nontrivial but is treated in this section using the data obtained from the tests presented herein.

439 Figure 17 shows the time-history of midspan deflections for slabs #1, #4, and #5 all of which
440 failed due loss of anchorage. While deflections at an early stage of the test were governed by
441 thermal bowing of the test specimens, the observed increase in the rate of midspan deflection
442 slope is thought to be linked to loss of anchorage (i.e. tendon slip).

443 Table 3 shows (for slabs #1, #4, and #5) the time from the start of the test, the temperature of
444 the CFRP tendons at midspan and 200 mm from the end of the slab for the following events:

- 445 • *A clear increase in the rate of midspan vertical displacement was observed* – This occurs
446 when the temperature of CFRP tendons at midspan was about 310°C (refer to Table 3).
447 The temperature of the CFRP tendons 200 mm from the end of the slab at this moment
448 was about 70-78°C for the 45 mm thick slabs (slabs #1 and #4), and 124°C for the 60
449 mm thick slab (Slab #5).
- 450 • *The first longitudinal cracks were observed at the unexposed surface* – This occurs when
451 temperature of the CFRP tendons at midspan was between 320 and 390°C (refer to
452 Figure 15), regardless of the temperature in the unheated overhangs (e.g. 200 mm from
453 the end of the slab, refer to Figure 16). Longitudinal splitting cracks were first observed
454 at the unexposed surface (i.e. top surface), near the midspan region (see Figure 20).
- 455 • *Failure occurred (i.e. collapse)* – The midspan temperature of the CFRP tendon at
456 failure of the slabs was higher for slabs that incorporated CFRP grids within the
457 anchorage zones. Slab #1, which had no CFRP grids, failed when the temperature of the
458 CFRP tendons at midspan was 459°C, while slabs #4 and #5, both of which included
459 CFRP grids, failed when the temperature of the CFRP tendons at midspan was 594°C

460 and 597°C, respectively. It is noteworthy that despite slabs #4 and #5 having depths of
 461 45 and 60 mm, respectively, their failure occurred when the temperature of the CFRP
 462 tendons at midspan was essentially the same.

463 The increase in midspan vertical displacement, appearance of the first longitudinal splitting
 464 crack, and failure of the slabs were apparently unrelated to the temperature of the CFRP
 465 tendons in the unheated overhangs.

466 **Table 3 – Time from the start of the test, the temperature of the CFRP tendons at midspan and 200 mm**
 467 **from the end of the slab when: (1) a clear increase in the rate of midspan vertical displacement was**
 468 **observed; (2) the first longitudinal crack was observed at the unexposed surface (i.e. the top surface); and**
 469 **(3) at failure for Slabs #1, #4, and #5.**

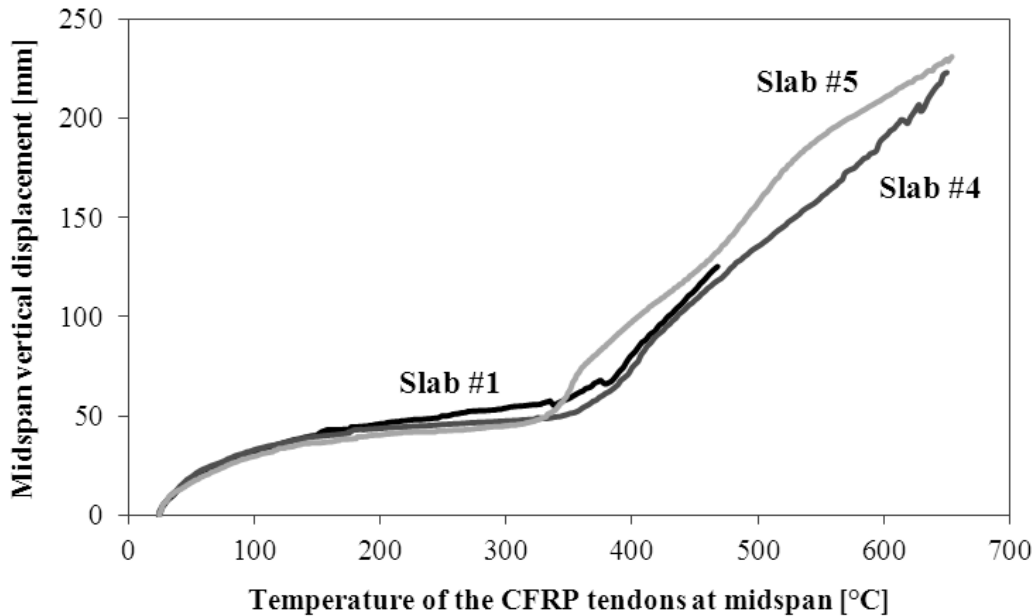
Slab #	Increase in the rate of midspan vertical displacement			First longitudinal splitting crack			Failure (i.e. structural collapse)		
	Time	Midspan	Unheated overhang	Time	Midspan	Unheated overhang	Time	Midspan	Unheated overhang
	[mm' ss'']	[°C]	[°C]	[mm' ss'']	[°C]	[°C]	[mm' ss'']	[°C]	[°C]
1	28' 00"	315°C	70°C	28' 40"	322°C	72°C	42' 01"	459°C	102°C
4	21' 24"	310°C	78°C	26' 16"	376°C	94°C	50' 27"	594°C	165°C
5	38' 00"	309°C	124°C	50' 40"	390°C	153°C	93' 04"	597°C	246°C



470
 471 **Figure 20 – Longitudinal splitting cracks at the unexposed surface of Slab #4 shortly before failure.**

472 Figure 18 shows draw-in measurements for CFRP tendons in Slab #1, evidencing that draw-
473 in initiated 16 minutes from the start of the test; at both the active and passive end of the slab.
474 Thereafter, draw-in progressively increased only at the active end up to 30 minutes from the
475 start of the start when a sudden increase in draw-in was measured at the passive end; around
476 the time at which an increase in the rate of midspan vertical displacement was observed for
477 Slab #1 (refer to Figure 17).

478 Interestingly, the time-history of midspan vertical displacement directly correlates with the
479 temperature of the CFRP tendons at midspan (see Figure 21), rather than temperature in the
480 unheated overhangs. This physical mechanism is thought to be associated with heat-induced
481 reduction for strength and stiffness of the epoxy resin within CFRP tendons; since the epoxy
482 resin is essential for anchorage to be maintained [4], and moreover for preserving interaction
483 and stress transfer between individual carbon fibres. Thermogravimetric analysis performed
484 by the authors on these particular CFRP tendons showed that decomposition of the epoxy
485 resin rapidly initiates at around 290°C [4]; in accordance with the temperature of the CFRP
486 tendons at midspan for which an increase in midspan vertical displacement was observed
487 (refer to Figure 21).



488

489

Figure 21 – Variation of midspan vertical displacement with temperature of the CFRP at midspan.

490 6.3 Influence of varying parameters

491 The following observations can be made regarding the influences of the various parameters
 492 investigated in the furnace test presented herein:

- 493 • *Concrete mix* – Mix B has a lower risk of heat-induced concrete spalling than Mix A,
 494 despite the fact that Mix A incorporated a higher dose of 2.0 kg of PP fibres (3 mm long)
 495 per m³ of concrete (as compared with 1.2 kg of 6 mm long PP fibres for Mix B). This
 496 suggests that not only PP fibre dose, as prescribed by most design guidelines (e.g. [13]),
 497 but also the length of the individual PP fibres has an influence on the effectiveness of PP
 498 fibres effectiveness at mitigating spalling; the current (limited) study therefore supports
 499 the use of 6 mm long fibres, although additional research is needed to corroborate this
 500 result.
- 501 • *Overall slab thickness* – The fire resistance of CFRP prestressed HPSCC slabs is directly
 502 associated to the overall slab thickness, with thicker slabs (unsurprisingly) having higher

503 fire resistances. The above is only valid when the slabs' failure mechanism is driven by
504 loss of anchorage rather than heat-induced concrete spalling. The positive influence
505 given by the slab thickness (hence concrete cover to the reinforcement) is fundamental to
506 the fire safety of concrete structural elements reinforced with steel or FRP [38].

507 • *The presence of CFRP grids within the anchorage zones* – For the CFRP prestressed
508 HPSCC slabs that failed due to loss of anchorage rather than spalling, the presence of
509 CFRP grids within the anchorage zones appears to increase the anchorage resistance of
510 the prestressed CFRP tendons; hence the overall fire resistance of slabs.

511 7 CONCLUSIONS

512 Recognizing that it is challenging to draw categorical conclusions on the basis of a limited
513 number of large-scale tests on CFRP prestressed HPSCC slabs simultaneously tested during a
514 furnace test, the following conclusions can be drawn on the basis of the data and analysis
515 presented in this paper:

516 • The fire resistance of CFRP prestressed HPSCC slabs during a standard fire resistance
517 test is influenced by the occurrence of heat-induced concrete spalling, and if no spalling
518 occurs, by loss of anchorage.

519 • Although all five test specimens were tested simultaneously and exposed to the same
520 notional time-history of temperature inside the furnace, variability was observed in the
521 time-history of through-thickness temperatures for essentially identical slabs. This
522 demonstrates the relatively poor, although 'test standard compliant', homogeneity of the
523 thermal loading imposed during a standard furnace test [32]. Interestingly, more rapid
524 through-thickness temperature increases were measured for slabs at the centre of furnace,
525 relative to those near its walls.

526 Relevant to the failure of slabs induced by the occurrence of heat-induced concrete spalling,
527 the following conclusions can be made:

- 528 • Failure of slabs #2 and #3 was driven by the occurrence of a single explosive spalling
529 event leading to sudden failure.

- 530 • The occurrence of heat-induced concrete spalling appears to be subtly influenced by the
531 time-history of through-thickness temperature within a concrete slab. Comparison of
532 temperature measurements recorded for slabs #1, #2, and #3 (all Mix A) indicated an
533 influence of time-history of through-thickness temperatures on the occurrence of heat-
534 induced concrete spalling. More rapid through-thickness temperature increases were
535 measured for slabs #2 and #3, which spalled at 12 and 22 minutes, respectively.

- 536 • Results suggest that a lower risk of spalling exists for slabs cast with Mix B (containing
537 1.2 kg/m^3 of 6 mm long PP fibres) than for those cast with Mix A (2.0 kg/m^3 of 3 mm
538 long PP fibres). This may be related to the short PP fibres (3 mm long) included in Mix
539 A being less effective in mitigating heat-induced concrete spalling. It is noteworthy that
540 existing European (and other) design guidelines for concrete in fire [13] prescribe the
541 inclusion of 2 kg/m^3 of monofilament PP fibres to ‘avoid’ spalling; this is clearly
542 indefensible based on the tests presented herein. Furthermore, these guidelines provide
543 no guidance on the required PP fibre diameter or length.

544 Relevant to failure of slabs induced by loss of anchorage:

- 545 • Whilst no attempt was made to individually identify the influence of thermo-mechanical
546 bond degradation versus thermo-mechanically induced longitudinal splitting cracking on
547 the loss of anchorage in CFRP prestressed HPSCC slabs, the tests confirmed that a
548 combination of both mechanisms is probably relevant.

549 • Irrespective of all design parameters assessed in this study, loss of anchorage appeared to
550 begin when the temperature at the lower edge of a central CFRP tendon at midspan was
551 in the range of 310°C, regardless of the temperature at the unheated overhangs. This
552 confirms the potential triviality of prescribing an unheated overhang length for the fire
553 resistance design of precast CFRP prestressed HPSCC slabs [10]. The precise reasons for
554 this remain unknown, although test results suggest influences of both longitudinal
555 thermal conduction (along and inside the CFRP tendons) and/or differential thermal
556 expansion (transverse to the tendon).

557 • The presence of CFRP grids within the anchorage zones appeared to increase the time-
558 to-failure for slabs that failed due to loss of anchorage. Slabs #4 and #5, which
559 incorporated CFRP grids, failed when the temperature at the bottom of the CFRP tendon
560 at midspan was at about 600°C, while it occurred at 450°C for Slab #1 which did not
561 incorporate grids. Increase in fire resistance is thought to be associated with increased
562 longitudinal splitting crack resistance and confining action provided by concrete (and
563 CFRP grids) in the anchorage zones.

564 The current study reveals some of the inadequacies of using standard furnace tests for
565 carefully investigating the fire resistance of CFRP prestressed HPSCC slabs (or similarly
566 novel or highly optimized structural elements). The high risk of heat-induced concrete
567 spalling and the complexities associated with loss of anchorage, both of which are relevant to
568 the fire behaviour of CFRP prestressed HPSCC slabs, are difficult to be rationally
569 investigated with a low number of test specimens, despite considerable instrumentation
570 during testing. A proper understanding of the response of these elements is needed before
571 they can be designed and implemented with confidence; this is unlikely to be achieved by
572 performing additional standard fire resistance tests. Conversely, what is needed is scientific

573 understanding of the thermal and mechanical fire behaviour of these elements at the material,
574 member, and system levels; this can be accomplished using a range of conventional and
575 bespoke test methods and procedures, many of which are now being used by the authors (e.g.
576 [11]).

577 **ACKNOWLEDGEMENTS**

578 The authors would like to thank SACAC Schleuderbetonwerk AG, Empa, and The University
579 of Edinburgh, and in particular Lukas Bäurle, Nunzio Spano, Thomas Hofer, Marcel Steiner,
580 Angelo Demont, and Mauricio Fuentes. This research was partially funded by Empa, the
581 BRE Centre for Fire Safety Engineering at The University of Edinburgh, and The Royal
582 Society of Edinburgh. Arup and the Royal Academy of Engineering are gratefully
583 acknowledged for their ongoing support of Arup Prof Bisby.

584 **NOTATION**

585	A_c	concrete cross section area
586	A_{CFRP}	CFRP tendons cross section area
587	E_c	elastic modulus of concrete
588	E_{CFRP}	elastic modulus of CFRP tendons
589	ε_c^{SR}	concrete strains due to shrinkage
590	$\Delta\sigma_p^{Total}$	total prestressing losses
591	$\Delta\sigma_p^{ES}$	prestressing losses due to elastic shortening of concrete
592	$\Delta\sigma_p^{SR}$	prestressing losses due to shrinkage of concrete
593	$\Delta\sigma_p^{CR}$	prestressing losses due to creep of concrete
594	$\sigma_{c,bottom}$	normal stress in concrete at the bottom fibre of slab
595	$\sigma_{c,0}$	initial normal stress in concrete

596	$\sigma_{CFRP,0}$	initial normal stress in CFRP tendons
597	$\sigma_{c,creep}$	normal stress in concrete after creep
598	$\sigma_{CFRP,est}$	initial prestressing level of the CFRP tendons during testing
599	φ_c	concrete creep coefficient
600	φ_{CFRP}	CFRP tendon-concrete bond creep coefficient
601		

602 **REFERENCES**

- 603 [1] Terrasi G.P. Prefabricated thin-walled structural elements made from HPC prestressed
604 with pultruded carbon wires. Proceedings of the 8th *International Symposium on Fibre*
605 *Reinforced Polymer Reinforcement for Concrete Structures*, Patras, Greece, 2007, 10
606 pp.
- 607 [2] Terrasi G.P., Battig G., and Bronnimann R. Pylons made of high-strength spun concrete
608 and prestressed with carbon fibre reinforced plastic for high power transmission lines.
609 *International Journal of Materials and Product Technology*, 2002, 17 (1-2), 32-45.
- 610 [3] Seica M.V. and Packer J.A. FRP Materials for the Rehabilitation of Tubular Steel
611 Structures, for Underwater Applications. *Composite Structures*, 2007, 80 (3), 440-450.
- 612 [4] Maluk C., Bisby L., Terrasi G.P., Hugi E., and Green M. Bond strength degradation for
613 CFRP and steel reinforcing bars in concrete at elevated temperature. *American*
614 *Concrete Institute Special Publication on Advances in Fire Design of Concrete*
615 *Structures (ACI SP-297)*, 2011, 36 pp.
- 616 [5] Kodur V.K.R. and Baingo D. Fire Resistance of FRP reinforced concrete slabs. *Institute*
617 *for Research in Construction (internal report)*, 1998, 44 pp.
- 618 [6] Kodur V.K.R. and Bisby L.A. Evaluation of Fire Endurance of Concrete Slabs
619 Reinforced with Fiber-Reinforced Polymer Bars. *Journal of Structural Engineering*,
620 2005, 131 (1), 34-43.

- 621 [7] Abbasi A. and Hogg P.J. Fire Testing of Concrete Beams with Fibre Reinforced Plastic
622 Rebar. *Composites Part A: Applied Science and Manufacturing*, 2006, 37 (8), 1142-
623 1150.
- 624 [8] Nigro E, Cefarelli G., Bilotta A., Manfredi G., and Cosenza E. Fire resistance of
625 concrete slabs reinforced with FRP bars. Part I: Experimental investigations on the
626 mechanical behavior. *Composites Part B: Engineering*, 2011, 42 (6), 1739-1750.
- 627 [9] Rafi M.M. and Nadjai A. Fire Tests of Hybrid and Carbon Fiber-Reinforced Polymer
628 Bar Reinforced Concrete Beams. *ACI Materials Journal*, 2011, 108 (3), 252-260.
- 629 [10] Terrasi G.P., Bisby L., Barbezat M., Affolter C., and Hugi, E. Fire Behavior of Thin
630 CFRP Pretensioned High-Strength Concrete Slabs. *Journal of Composites for*
631 *Construction*, 2012, 16 (4), 381–394.
- 632 [11] Maluk C. Development and Application of a Novel Test method for Studying the Fire
633 Behaviour of CFRP Prestressed Concrete Structural Elements. Ph.D Thesis, *The*
634 *University of Edinburgh*, UK, 2014, 473 pp.
- 635 [12] Bailey C.G. and Khoury G.A. Performance of Concrete Structures in Fire – An In-
636 depth Publication on the Behaviour of Concrete in Fire. *MPA - The Concrete Centre*,
637 Ruscombe Printing Ltd, Reading, UK, 2011, 187 pp.
- 638 [13] CEN. Eurocode 2: Design of Concrete Structures – Parts 1-2: General Rules –
639 Structural Fire Design (EN 1992-1-2). *European Committee for Standardization*,
640 *Brussels*, 2004, 100 pp.
- 641 [14] CCAA. Fire Safety of Concrete Buildings. *Cement Concrete & Aggregates Australia*
642 *(CCAA)*, 2013, 33 pp.

- 643 [15] Katz A. and Berman N. Modeling the Effect of High Temperature on the Bond of FRP
644 Reinforcing Bars to Concrete. *Cement and Concrete Composites*, 2000, 22 (6) 433-443.
- 645 [16] Bisby L.A. and Kodur V.K.R. Evaluating the Fire Endurance of Concrete Slabs
646 Reinforced with FRP Bars: Considerations for a Holistic Approach. *Composites Part B:
647 Engineering*, 2007, 38 (5-6), 547-558.
- 648 [17] Katz A. Bond Mechanism of FRP Rebars to Concrete. *Materials and Structures*, 1999,
649 32 (10), 761-768.
- 650 [18] Morley P.D. and Royles R. The Influence of High Temperature on the Bond in
651 Reinforced Concrete. *Fire Safety Journal*, 1980, 2 (4), 243-255.
- 652 [19] Bednarek Z. and Ogrodnik P. Testing steel-concrete bond in fire conditions.
653 Proceedings of the 9th *International Conference Modern Building Materials, Structures
654 and Techniques*, Vilnius, Lithuania, 2007, 1152–1158.
- 655 [20] Haddad R.H., Al-Saleh R.J., and Al-Akhras N.M. Effect of Elevated Temperature on
656 Bond Between Steel Reinforcement and Fiber Reinforced Concrete. *Fire Safety
657 Journal*, 2007, 43 (5), 334-343.
- 658 [21] Pothisiri T. and Panedpojaman P. Modeling of Mechanical Bond–Slip for Steel-
659 Reinforced Concrete Under Thermal Loads. *Engineering Structures*, 2013, 48 (March),
660 497-507.
- 661 [22] Aiello M.A., Leone M., and Pecce M. Bond Performances of FRP Rebars-Reinforced
662 Concrete. *Journal of Materials in Civil Engineering*, 2007, 19 (3), 205-213.

- 663 [23] Wang Y.C., Wong P.M.H., and Kodur V.K.R. An Experimental Study of the
664 Mechanical Properties of Fibre Reinforced Polymer (FRP) and Steel Reinforcing Bars
665 at Elevated Temperatures. *Composite Structures*, 2007, 80 (1), 131-140.
- 666 [24] ACI. Prestressing Concrete Structures with FRP Tendons (ACI 440.4R-04). *American*
667 *Concrete Institute*, Farmington Hills, MI, US, 2004, 35 pp.
- 668 [25] FIB. FRP Reinforcement for RC Structures. *Technical report prepared by Task Group*
669 *9.3 FRP (Fibre Reinforced Polymer) reinforcement for concrete structures*. Lausanne,
670 Switzerland, 2006, 157 pp.
- 671 [26] CNR. Guide for the Design and Construction of Concrete Structures Reinforced with
672 Fiber-reinforced Polymer Bars (CNR-DT 203/2006). *National Research Council*,
673 Rome, Italy, 2007, 39 pp.
- 674 [27] Maluk C., Bisby L., and Terrasi G.P. High temperature compatibility of CFRP versus
675 steel reinforcement for concrete. *American Concrete Institute Special Publication*
676 *Towards Sustainable Infrastructure with Fiber Reinforced Polymer Composites (ACI*
677 *SP-440)*, 2015. (*in press*)
- 678 [28] Aiello M.A. Concrete Cover Failure in FRP Reinforced Beams under Thermal Loading.
679 *Journal of Composites for Construction*, 1999, 3 (1), 46-52.
- 680 [29] Aiello M.A., Focacci F., and Nanni A. Effects of Thermal Loads on Concrete Cover of
681 Fibre-Reinforced Polymer Reinforced Elements: Theoretical and Experimental
682 Analysis. *ACI Materials Journal*, 2001, 98 (4), 332-339.
- 683 [30] Masmoudi R., Zaidi A., and Gérard P. Transverse Thermal Expansion of FRP Bars
684 Embedded in Concrete. *Journal of Composites for Construction*, 2005, 9 (5), 377-387.

- 685 [31] Abdalla H. Concrete Cover Requirements for FRP Reinforced Members in Hot
686 Climates. *Composite Structures*, 2006, 73 (1), 61-69.
- 687 [32] CEN. Eurocode: Fire Resistance Tests – Part 1: General Requirements (EN 1363-
688 1:2012). *European Committee for Standardization*, Brussels, 2012, 56 pp.
- 689 [33] CEN. Eurocode: Testing Hardened Concrete – Part 6: Tensile Splitting Strength of Test
690 Specimen (EN 12390-6:2009). *European Committee for Standardization*, Brussels,
691 2009, 14 pp.
- 692 [34] CEN. Eurocode: Testing Fresh Concrete – Part 8: Self-compacting Concrete – Slump-
693 Flow Test (EN 12350-8:2010). *European Committee for Standardization*, Brussels,
694 2010, 14 pp.
- 695 [35] Terrasi G.P., Affolter C., and Barbezat M. Numerical Optimization of a Compact and
696 Reusable Pre-tensioning Anchorage System for CFRP Tendons. *Journal of Composites
697 for Construction*, 2010, 15 (2), 126–135.
- 698 [36] Empa. Concrete Shrinkage and Creep Strain Measurements (Bestimmung des Schwind-
699 und Kriechwertes). Internal report from the *Swiss Federal Laboratories for Materials
700 Science and Technology (Empa)*, Dübendorf, Switzerland, 2008, 4 pp.
- 701 [37] Usmani A.F., Rotter J.M., Lamont S., Sanad A.M., and Gillie M. Fundamental
702 Principles of Structural Behaviour Under Thermal Effects. *Fire Safety Journal*, 2001,
703 36 (8), 721-744.
- 704 [38] Buchanan A.H. *Structural Design for Fire Safety*. John Wiley & Sons Ltd., West
705 Sussex, UK, 2001, 448 pp.